

Mechanical Analysis of Fault Slip Rate Sites within the San Gorgonio Pass Region, Southern California USA

J. Hatch¹, M. Cooke^{1,*}, and H. Elston¹

5

¹Department of Geosciences, University of Massachusetts, Amherst, USA

*Corresponding author:

10 *This is a non-peer reviewer preprint that was submitted to Seismica on July 15, 2022. Please note that subsequent versions of this manuscript may have slightly different content. If accepted, the final version of this manuscript will be available via the Peer-reviewed Publication DOI link on the right hand side of this web page.*

15 **Author ORCIDs, email and twitter handle**

A. Jennifer Hatch: 0000-0001-8877-2176 | jennbeyer6@gmail.com

B. Michele Cooke: 0000-0002-4407-9676 | cooke@umass.edu | @geomechCooke

C. Hanna Elston: 0000-0002-2420-5241 | helston@umass.edu | @HannaElston

Author contributions

20 Conceptualization: J. Hatch, M. Cooke

Formal Analysis: J. Hatch, M Cooke, H. Elston

Writing – original draft: J. Hatch, M. Cooke

Writing – review & editing: M. Cooke, J. Hatch, H. Elston

25 **Abstract**

Crustal deformation models show incompatibility between inferred fault geometry and geologic slip rates where model and geologic slip rates disagree. We do not know if the impact of these incompatibilities is limited to near sites or have wider effect on the fault system deformation. Here, we investigate the roles of structural position of sites and uncertainty of slip rates using one suite of mechanical models that limits the dextral slip rates to within the range of observed slip rates at the sites of geologic investigations and another suite that explores the impact of each slip rate site on each other and on the nearby fault system. The suites of models employ two viable configurations for the southern San Andreas fault: with and without an active northern slip pathway around the San Gorgonio Pass. While the *Active Northern Pathway* model has greater mismatch to geologic slip rates < 16ka, it produces lesser off-fault deformation than the *Inactive Northern Pathway* model. The impact of strike-slip rate sites on the system depends on their structural positions. Sites along segmented faults may have lesser impact than either sites along the same fault segment or sites at fault branches. Consequently, inaccuracies in the slip rates used for seismic hazard assessment may have differing impacts depending on location of the slip rates. Fault branches along strike-slip faults warrant detailed investigation because these areas have high spatial variability of slip rate and accrue nearby off-fault deformation, affecting our ability to accurately assess seismic hazard of the region.

Non-technical summary

Earthquake hazard assessments rely on observations from the field and geophysical data that provide fault slip rate estimates at specific sites and inform active fault shape within the crust; however, uncertainty remains for both slip rate and shape. Numerical models that simulate slip along 3D faults of the southern San Andreas fault system produce slip rates that match some but not all field observations. At the mismatched sites, the model fault shape is incompatible with slip rates indicating inaccuracies in the fault shape and/or slip rate. We investigate how uncertainty or inaccuracy of a slip rate at one site impacts other sites and the overall fault system. Sites that are nearby each other have the greatest impact on each other and sites along fault branches have high impact on the fault system. This means that uncertainties in slip rates used for earthquake hazard assessment may have differing impacts depending on the slip rate site's location within the fault network. Hazard assessments can benefit from additional data along fault branches. Continuing to measure how fast faults are slipping in the field and reduce the uncertainty of such measurements will increase the accuracy of earthquake hazard assessments.

1. Introduction

The southern San Andreas fault forms a restraining stepover in the San Gorgonio Pass region (SGPr), characterized by multiple active fault strands and complex interactions (Figure 1). Due to the lack of large ground rupturing earthquakes during the span of the seismic catalog (e.g., Yang, Hauksson, & Shearer, 2012 and subsequent updates), the activity and subsurface geometry of the San Andreas fault through the SGPr remains uncertain. The available geologic observations and geophysical subsurface data allow for conflicting interpretations of fault geometry in many portions of the SGPr.

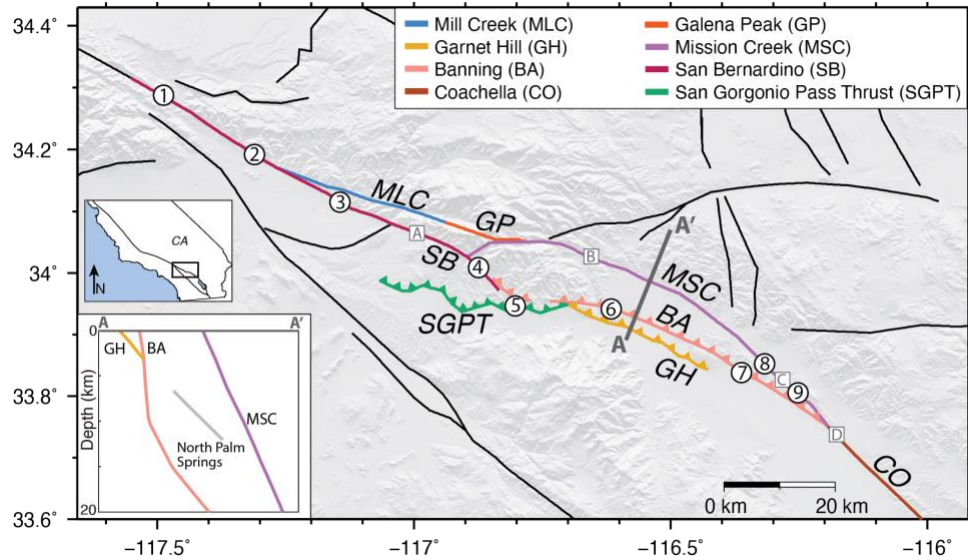


Figure 1. The surface traces of modeled faults overlain on a digital elevation map (DEM). Different trace colors indicate the specific fault segments. Numbers in circles show the location of slip rate sites that we use to constrain the model slip rate. Letters in squares the location of slip rate sites that we do not use to constrain the model slip rate. The bottom left inset shows the cross-section profile along the A-A' line (dark gray). The top left inset shows the region of interest (black rectangle) on a map of southern California. Table 1 lists the name and citation for all the slip rate sites. BA – Banning, CO – Coachella, GH – Garnet Hill, GP – Galena Peak, MLC – Mill Creek, MSC – Mission Creek, SB – San Bernardino, SGPT – San Gorgonio Pass Thrust.

65 For example, on-going debate centers on the relative activity of the Mill Creek and Mission
 Creek strands, which provide a northern path for rupture through the SGPr (Figure 2; Blisniuk et
 al., 2021; Fosdick & Blisniuk, 2018; Gold et al., 2015; Kendrick, Matti, & Mahan, 2015).
 Kendrick et al. (2015) used reconstructed drainage segments across the Mill and Mission Creek
 strands (site 6 in Figure 1) to show that both strands, while active in the past, have been inactive
 70 for ~ 100 ka. However, a provenance study in this same area by Fosdick and Blisniuk (2018)
 suggests that these strands are active. Farther to the east along the Mission Creek fault, two sites
 within 5 km of each other (sites 9 and 10; Figure 1) have slip rates that differ by >10 mm/yr;
 19.6 - 23.6 mm/yr at site 9 (Blisniuk et al., 2021) and 10-14 mm/yr at site 10 (Muñoz Zapata,
 2017). One approach for reducing active fault geometry uncertainty is to test plausible fault
 75 configurations by comparing results of alternative mechanical models with geologic slip rates,
 uplift, and/or geodetic data (e.g., Beyer, Cooke, & Marshall, 2018; Cooke & Dair, 2011;
 Fattaruso, Cooke, & Dorsey, 2014; Justin W. Herbert & Cooke, 2012). For example, Beyer et al.
 (2018) find that two among six plausible configurations of the San Andreas fault through the
 SGPr fit well the available geologic slip rates. One limitation of this forward modeling approach
 80 is that the explicit set up of the fault configurations does not inform the feasibility of alternatives
 outside of those tested or if the remaining inaccuracies have a small or large impact on the
 deformation of the fault system.

Crustal deformation models of plausible fault configurations inform the kinematic compatibility
 of the fault system and highlight regions that would benefit from further investigation. Kinematic

85 compatibility of a fault system describes how deformation is partitioned through the system (e.g.,
Gabrielov, Keilis-Borok, & Jackson, 1996; Hatem, Cooke, & Madden, 2015) and its analysis can
highlight regions where fault long term slip rates are incompatible with fault geometry. If
interpreted fault geometries and slip rates are kinematically compatible within an efficient fault
90 system, deformation will be accommodated as on-fault slip rather than off-fault deformation. In
contrast, if interpreted fault geometries and slip rates are kinematically incompatible, such as fast
slip rates through a sharp fault bend, deformation that cannot be effectively accommodated as
fault slip results in local off-fault deformation. High rates of off-fault deformation promote
reorganization of the fault system (e.g., Cooke, Toeneboehn, & Hatch, 2020; Fattaruso, Cooke,
Dorsey, & Housen, 2016) and suggest that the interpreted active fault geometry is incompatible
95 with the long term slip rate. Regions of high incompatibilities may benefit from additional data
to better characterize the local fault geometry or slip rate. Furthermore, while some fault
irregularities may only produce local off-fault deformation and persist throughout fault evolution
(Hatem, Cooke, & Toeneboehn, 2017), other incompatibilities between fault geometry and slip
rate may have great impact on slip rates throughout the fault system. By assessing the locations
100 along the fault system with the greatest influence on slip rates, we can better understand the
potential impact of uncertainties and inaccuracy on our seismic hazard estimates.

In this study, we use three-dimensional Boundary Element Method models that simulate
deformation over many earthquake cycles to investigate the kinematic compatibility of
interpreted fault geometry with interpreted slip rates through the San Gorgonio Pass region
105 (Figure 1). Rather than letting faults slip in response to tectonic loading as done with many
previous models (e.g., Beyer et al., 2018), here we prescribe geologic slip rates at the sites of the
investigation. This allows the models to incorporate both interpreted slip rates and fault geometry
at the same time so that we can assess their compatibility. To explore the impact of these
locations and slip rate uncertainties, we investigate a second suite of models that apply 1 mm/yr
110 to each of the sites independently to assess how slip at different slip rate sites impact slip on the
fault system due to variations in their structural position.

2. Geometry and slip rates of the southern San Andreas fault

Within the San Gorgonio Pass region (SGPr), the southern San Andreas fault forms a left-
stepping restraining bend and becomes geometrically complex, with multiple active fault strands
115 and a complex slip history (Matti & Morton, 1993; Figure 1; Matti, Morton, & Cox, 1985). In
this section, we describe the interpreted geometry and records of recent slip rate along both the
southern and northern strands of the San Andreas fault. The San Andreas fault geometry used in
this study primarily follows that of the Southern California Earthquake Center Community Fault
Model v. 5 (Plesch et al., 2007; Shaw et al., 2015) with exceptions noted below.

120 Dextral slip rates consistently decrease from north to south along the San Bernardino strand of
the San Andreas fault from Cajon pass to where the strand approaches the San Gorgonio Pass
Thrust. Near Cajon Pass, at Cajon Creek the San Bernardino strand shows 21-28 mm/yr slip
from ~14 ka geomorphic features (site 1: Weldon & Sieh, 1985). The next three sites to the south

125 constrain slip rates from offsets of 10-16 ka alluvial fans with 8.3-16 mm/yr at Badger Canyon
(site 2: McGill, Owen, Weldon, Kendrick, & Burgette, 2021), 7-17 mm/yr dextral slip at Plunge
Creek (site 3: McGill, Owen, Weldon, & Kendrick, 2013) and 14-25 mm/yr at Wilson Creek (site
A: Harden & Matti, 1989). The fan age at Wilson Creek site is an estimate rather than a
measurement, which results in a large slip rate range. Note: sites with slip rates that are either not
130 well constrained or older than 16 ky are given a letter site name rather than a number and are not
used to constrain the models. The southernmost slip rate site on the San Bernardino strand has 4-
12 mm/yr slip rate recorded by offset of a ~4 ka alluvial fan at Burro Flats (site 4: Orozco, 2004).

Active slip along the southern pathway of the San Andreas fault within the SGPr occurs along
the San Gorgonio Pass thrust, Garnet Hill strand, and Banning strand (Figure 1). The San
Gorgonio Pass thrust is a north-dipping thrust fault that intersects the Earth's surface with a
135 scalloped trace (Matti & Morton, 1993; e.g., Matti et al., 1985; Yule & Sieh, 2003). The San
Gorgonio Pass thrust has offset ~8ka terraces to record a dextral slip rate of 5.7 (+2.7 -1.5)
mm/yr at Millard Canyon (site 5: Heermance & Yule, 2017). To the east of Millard Canyon, the
north-dipping Garnet Hill and Banning strands are nearly parallel in strike and have several
different interpreted subsurface geometries (Fuis et al., 2017; Plesch et al., 2007; Yule & Sieh,
140 2003). For this study, we follow the interpretations of Fuis et al. (2017) that the Garnet Hill
strand is only active in the footwall of the Banning strand (Figure 1). While the Garnet Hill
strand does not offer geomorphic features that can provide slip rate estimates, the parallel
Banning strand offsets ~6 ka alluvial fans at both its western and eastern ends. The fan at Painted
Hills records 3.9-4.9 mm/yr dextral slip (site 6: Gold et al., 2015) and the fan at Washington
145 Street, near the intersection of the Banning strand with Mission Creek strand, records 1.5-3.5
mm/yr dextral slip (site 7: Blisniuk et al., 2021).

The northern slip pathway of the San Andreas fault consists of the Mill Creek, Galena Peak, and
Mission Creek strands (Figure 1). While the northern pathway was active in the past and served
as the primary structure of the San Andreas fault in this region, recent activity of these vertical
150 faults are under debate (e.g., Beyer et al., 2018; Blisniuk et al., 2021; Fosdick & Blisniuk, 2018;
Kendrick et al., 2015). Here, we include the Galena Peak strand as part of the northern pathway
as it connects the Mill Creek strand and western part of the Mission Creek strand (e.g., Dibblee,
1964; Kendrick et al., 2015; Matti & Morton, 1993). This active fault configuration allows slip to
by-pass Upper Raywood Flats where Kendrick et al. (2015) see no evidence of slip in the past
155 100 ka. Beyer et al. (2018) found that among six plausible configurations of the San Andreas
fault strands, the configuration that includes Galena Peak matches the available geologic slip
rates as well as the model without an Active Northern Pathway for slip through the San Gorgonio
Pass.

160 Researchers report differing degrees of recent activity along the Mill Creek and Mission Creek
strands west of the Galena Peak strand to the location just west of the A-A' transect within Figure
1. One study of the Mission Creek alluvial complex suggests that neither the Mission Creek nor
Mill Creek faults have slipped at this location for 100 ka (site B: Kendrick et al., 2015). In

contrast, a sedimentary provenance study of modern drainages just a few kilometers away suggests that the Mission Creek fault may accommodate most of the deformation in the region (Fosdick & Blisniuk, 2018). To the east of the A-A' transect within Figure 1, the Mission Creek strand shows abundant evidence for slip but with a wide range of dextral slip rates. Within the Indio Hills, channel offsets at Pushawalla Canyon show high dextral slip rates of 19.6-23.6 mm/yr over the past ~90 ka (site C: Blisniuk et al., 2021), consistent with active slip along the northern pathway through the SGPr. However, these channels do not record recent slip rates within the past 16 ka. A few kilometers south from Pushawalla Canyon at Three Palms, a young 2.6-6.4 ka alluvial fan shows much lower slip rate of 9-14 mm/yr dextral slip along the Mission Creek strand (site 9: Muñoz Zapata, 2017). A few kilometers north of Pushawalla, offset channels trenched across the Mission Creek fault at Thousand Palms recorded two slip events within the last ~500 years that give slip rates of 2-6 mm/yr (site 8: Fumal, Rymer, & Seitz, 2002). Because trenches can miss expressions of slip along fault splays outside of the trench, we consider this a minimum slip rate for the Thousand Palms site.

The Banning and Mission Creek strands merge into the Coachella segment of the San Andreas fault just south of the Indio Hills (Figure 1). The Coachella segment dips to the northeast (e.g., Fattaruso et al., 2014; Fuis et al., 2017; Lin, 2013; Lindsey & Fialko, 2013) and continues southward from the Indio Hills to the eastern shore of the Salton Sea. Near the Indio Hills, the Mission Creek strand and the Coachella segment dip 5-10 degrees shallower in the Fuis-based models than in the CFM-based models due to changes in the geometry of the Banning strand. This geometry honors the interpretations of Fuis et al. (2017) for the Banning, Garnet Hill and Mission Creek strands to the north of Palm Springs and for the Coachella segment to the south of the Indio Hills. Just south of the junction with the Banning and Mission Creek, the Coachella segment shows evidence from ~50ka alluvial fans for a preferred rate of 14-17 mm/yr at Biskra Palms (site D: Behr et al., 2010).

Site	Name	age	Dextral slip rate (mm/yr)	citation	Used to constrain model slip rate in this study?
1	Cajon Creek	~14 ka	21-28	Weldon & Sieh, 1985	yes
2	Badger Canyon	13-15 ka	11.8 ^{+4.2} / _{.3,5}	McGill et al. 2021	yes
3	Plunge Creek	10.5 ka	6.3-18.5	McGill et al., 2013	yes
A	Wilson Creek	~14 ka	14-25	Harden & Matti, 1989	no; non-robust age
4	Burro Flats	~4 ka	4-12	Orozco et al., 2004	yes
5	Millard Canyon	~8ka	5.7 ^{+2.7} / _{.1,5}	Heermance & Yule, 2017	yes
6	Painted Hills	~6 ka	3.9-4.9	Gold et al., 2015	yes

7	Washington St.	~6 ka	1.5-3.5	Blisniuk et al. 2021	yes
B	Mission Creek Alluvial Fan Complex	>~100ka	0 or > 0	Kendrick et al., 2015; Fosdick & Blisniuk, 2018	not constrained in Active Northern Pathway model
8	Thousand Palms	~500 years	2-6	Fumal et al., 2002	Lower limit
C	Pushawalla Canyon	~90 ka	19.6-23.6	Blisniuk et al. 2021	no; age > 16ka
9	Three Palms	2.6-6.4 ka	9-14	Munoz et al., 2016	yes
D	Biskra Palms	~50ka	14-17	Behr et al., 2010	no; age > 16 ka

Table 1: Data from geologic slip rate sites

3 Methods

190 We evaluate the impact of slip rates and sites along faults within the San Gorgonio Pass region using Poly3D, a quasi-static, three-dimensional boundary element code. Poly3D calculates stresses and displacements throughout the model by solving the relevant equations of continuum mechanics (Crider & Pollard, 1998; Thomas, 1993). In addition to detailed three-dimensional representation of faults described in section 2, the models incorporate the San Jacinto fault and
195 faults of the Eastern California Shear Zone based on the Community Fault Model version 5 (Figure 2). Modifications to the Community Fault Model representation have improved the match of model slip rates to geologic slip rates; we include these modifications of the Eastern California Shear Zone described by Herbert et al. (2014) and of the Coachella segment described by Fattaruso et al. (2014). We remesh the Community Fault Model for more uniform element
200 size and we iteratively refine the mesh to reduce model artifacts that arise when the faults slip.

For the mesh, faults are discretized into triangular elements that can replicate complex fault geometries within a linear-elastic and otherwise homogeneous half-space (Figure 2). Within the San Gorgonio Pass region, the average element size is ~4 km, allowing for the models to capture fault irregularities as small as ~10 km. Following Marshall et al. (2009), we extend the faults of
205 the CFM down to a horizontal basal crack that is freely slipping at 35 km depth to simulate distributed deformation below seismogenic depths. This adaptation allows us to simulate long-term deformation without the fault slip rates going to zero at the base of the CFM-defined faults. Furthermore, we do not consider impacts of heterogeneous and/or anisotropic rock properties. Over multiple earthquake cycles, fault geometry provides a first-order control on deformation
210 patterns (e.g., Dawers & Anders, 1995; Fay & Humphreys, 2005; Justin W. Herbert & Cooke, 2012).

Within the unconstrained models, the shear traction-free faults throughout the model slip freely in response to both the tectonic loading and fault interaction. Zero shear traction is consistent with low dynamic strength of faults during rupture (Di Toro, Hirose, Nielsen, & Pennacchioni,
215 2006; e.g., Goldsby & Tullis, 2011). Tectonic loading is prescribed far from the investigated

220 faults at the base of the model, following Herbert & Cooke (2012) to simulate plate motions that are geodetically constrained as 45-50 mm/yr at 320°-325° (e.g., DeMets, Gordon, & Argus, 2010). Following Beyer et al. (2018), we also implement an iterative technique that uses a correction ratio for successive iterations to ensure a uniform applied tectonic velocity parallel to the plate boundary (sides labeled I on Figure 2) and a linear gradient in the tectonic loading across the plate boundary (sides labeled II on Figure 2). This technique provides applied velocities that are within ~1% of the desired tectonic loading.

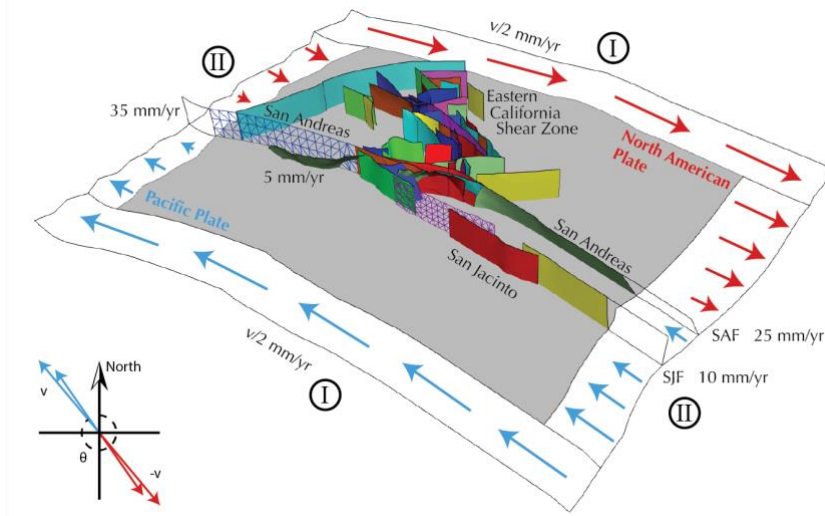


Figure 2. Oblique view of the model setup. Tectonic loading is prescribed far from the investigated faults at the boundaries of the model base. Zone of applied loading is much wider than shown here. Fault slip rates are prescribed at the distal end of faults that extend beyond the model boundaries. Faults within the model slip freely in response to both tectonic loading and fault interaction. A range of plate velocities and orientations account for uncertainty in tectonic loading. SAF - San Andreas fault; SJF - San Jacinto fault.

225 To prevent slip from artificially going to zero on faults that extend outside our model area (i.e., the San Andreas, San Jacinto, and Cucamonga-Sierra Madre fault systems), we prescribe slip rates to patches of these faults at the edge of our model. For the San Andreas fault, we apply 35 mm/yr dextral slip (Weldon & Sieh, 1985) at the northwestern edge of the model. At the southeastern edge of the model, we apply 25 mm/yr and 10 mm/yr dextral slip to the San Andreas and San Jacinto faults, respectively (e.g., Becker, Hardebeck, & Anderson, 2005; Fay & Humphreys, 2005; Meade & Hager, 2005; Sharp, 1981). Deformation within the SGPr is not significantly impacted by variations in the partitioning of slip rates between the San Andreas and San Jacinto faults at this model edge because slip rates primarily respond to interaction among complex faults within the San Gorgonio Pass region (Fattaruso et al., 2014). Finally, we apply 1.6 mm/yr reverse slip (McPhillips & Scharer, 2018) to the western edge of the modeled Cucamonga fault to account for deformation along the Sierra Madre fault, which is not included in our model.

Because of the ongoing debate on the recent activity of the Mill Creek strand, we assess two alternative active fault configurations. The first model considers the northern slip pathway

inactive through the SGPr; the model does not include the Mill Creek or Galena Peak strands and
240 only allows slip along the Mission Creek strand southeast of the transect A-A' on Figure 1. The
second model expands from the first fault configuration and additionally incorporates active Mill
Creek and Galena Peak strands as well as the entire Mission Creek strand (Figure 1). We refer to
these fault configurations as the *Inactive Northern Pathway* and the *Active Northern Pathway*
models.

245 3.2 Impact of slip rates and their uncertainty

To assess the impact of slip rates and their uncertainty on the fault system we compare the fault
slip rates and off-fault deformation of models with both unconstrained and constrained slip rates.
Within a first set of unconstrained models, we allow the faults in the model to slip freely in
response to tectonic loading and fault interaction. In a second set of constrained models, we limit
250 the slip rates at geologic sites within the models to within the geologic range. At each slip rate
site along the fault, the prescribed slip rate patch is ~2 km by 2 km, just below the surface trace
of the fault. Locations along the faults between the prescribed slip rate sites freely slip in
response to tectonic loading, fault interaction, and the effects of prescribed slip patches.

Because geologic investigations produce a range of possible slip rates, we allow for a variety of
255 slip rates at each site of geologic investigation in the model. In the absence of probability density
functions for the slip rates, we treat the geologic slip rate as having uniform ("box car")
probability within the published range. If the slip rates from the unconstrained model lie outside
of the geologic range, then we prescribe the slip rate at the site to be either the upper or lower
limit of the geologic slip rate range. If the slip rate in the unconstrained model is closer to the
260 upper bound then we prescribe this slip rate at the site, otherwise we prescribe the lower bound
slip rate at the site.

Because some sites have uncertain or debated recent slip rates, we either exclude them or limit
their role within the constrained models (Table 1). The alluvial fan age at the Wilson Creek site
uses qualitative soil chronology rather than modern age dating approaches (Harden and Matti,
265 1985). Because of this uncertainty, we include the slip rate for comparison but do not constrain
the model to fit this slip rate. We also exclude slip rate constraints on the Mission Creek strand at
the Mission Creek Alluvial Fan Complex within the *Active Northern Pathway* model due to on-
going debate of recent activity along this portion of the fault (Fosdick & Blisniuk, 2018;
Kendrick et al., 2015). The slip rate from the Thousand Palms site may not include nearby fault
270 strands (Fumal et al., 2002); we use the reported range as a lower limit only for dextral slip rates.
Two slip rates from the Pushawalla Canyon and Biskra Palms sites are based on > 60 ka alluvial
fans (Behr et al., 2010; Blisniuk et al., 2021). Because the activity among fault strands in the San
Gorgonio Pass has shifted over the past 100 ka, strands that were active 60 ka may have different
activity now. Laboratory experiments of restraining bends with similar geometry to the San
275 Andreas fault through the San Gorgonio Pass show that such bends are not stable fault
configurations (Cooke, Schottenfeld, & Buchanan, 2013; Hatem et al., 2015) and slip rates can

vary on time spans of ~50 ka (Elston, Cooke, & Hatem, 2022). For this reason, we only use slip rates from offset of features younger than ~16 ka to constrain the models.

280 We assess the kinematic incompatibility of the two fault configurations (*Inactive* and *Active Northern Pathway*) for both the unconstrained and constrained models by calculating maps of the off-fault net deformation rate, here defined as the sum of the vorticity rate and the divergence rate derived from the velocity field at the top surface of the model half-space. The vorticity captures the distortion along and off of faults while divergence captures dilatational strain. In
285 order to investigate the off-fault deformation, we exclude net strain rate information within 1 km from all active faults. We compare both the resulting off-fault strain rate pattern and the mean strain rate across the region to those of the unconstrained models. The spatial patterns of deformation reveal regions where geologic slip rates are incompatible with interpreted fault geometry, while average net strain rate provides a metric for the relative overall kinematic
290 compatibility of the system.

3.3. Assessing impact of each slip rate site on the system

For the analysis of kinematic compatibility, we constrain the sites together so that the models produce slip rates within the geologic bounds. While these results highlight regions of the model where fault geometry is incompatible with geologic slip rates, they do not inform the role of each
295 site on the slip distribution within the system. Due to their structural position, some sites may have a stronger influence on the fault system's slip rate than other sites. We assess the sensitivity of individual sites by exploring the response of the fault system to 1 mm/yr of dextral strike slip applied at each of the sites independently. The influence factors report the change in slip rate at all other sites due to the applied 1 mm/yr at each site. To assess the impact along stretches of
300 fault between the slip rate sites, we also calculate slip rate impact factors by integrating the slip along the fault system that results from applying 1 mm/yr at each site.

4 Results

Here, we present plots of fault slip rates and maps of off-fault deformation through the SGPr for an *Inactive Northern Pathway* and an *Active Northern Pathway* unconstrained and constrained
305 models. These two models represent different interpretations for fault activity in the region. Sites without reliable slip rates within the past 16k years (sites A, B, C and D) are not constrained within the models but are considered within the analysis of site impact. We discuss both the influence of each slip rate site on each other, as well as the regional impact of each slip rate site.

4.1 Surface slip rates through the San Gorgonio Pass region

310 Forward numerical models that simulate tectonic loading can provide slip rate estimates along the entire fault surface including at the sites of geologic slip rate investigations. Models for the San Andreas fault show dextral slip rates that vary along the fault strands through the SGPr. Figures 3A and 3B show the slip rate at the upper surface of the model for the unconstrained

315 models with and without an *Active Northern Pathway* for slip. For both models, the band shows the slip rates for the range of tectonic loading applied to the models.

In the model with *Inactive Northern Pathway* geometry (Figure 3a), the dextral slip rate along the San Bernardino strand (maroon) gradually decreases southward from Cajon Pass, with a small, stepped decrease in slip rate between Plunge Creek (site 3) and Wilson Creek (site A), where the San Gorgonio Pass Thrust (green) takes up some dextral slip. Dextral slip rate along the San Gorgonio Pass Thrust generally increases to the east to reach a maximum of ~6 mm/yr dextral slip near its intersection with the Banning strand (coral). Because strike-slip is partitioned between both the San Gorgonio Pass Thrust and a short active segment of the Banning strand that parallels the San Gorgonio Pass Thrust (Fig. 1), the dextral slip rate along the thrust varies along strike. The model produces a local low in dextral slip along the San Gorgonio Pass Thrust at Millard Canyon (site 5). Dextral slip on the Garnet Hill strand (beige) decreases to the east, where the fault trace ends just short of reaching the Coachella segment of the San Andreas fault (brown). In contrast, dextral slip on both the Banning strand and the active portion of the Mission Creek strand (purple) increase to the east to maximum values where these faults merge with the Coachella segment.

330 In the unconstrained *Active Northern Pathway* geometry (Figure 3b), the dextral slip rate along the San Bernardino strand decreases with distance from Cajon Pass, similar to slip rates of the *Inactive Northern Pathway* model, the dextral slip rate abruptly decreases between Badger Creek (site 2) and Plunge Creek (site 3), due to the transfer of dextral slip onto the Mill Creek strand (blue). Farther to the east, dextral slip of ~10 mm/yr along the Mill Creek strand continues onto the Galena Peak strand (orange). The dextral slip rates along the Mission Creek and Banning strands gradually increase to the southeast where these strands merge with the Coachella segment.

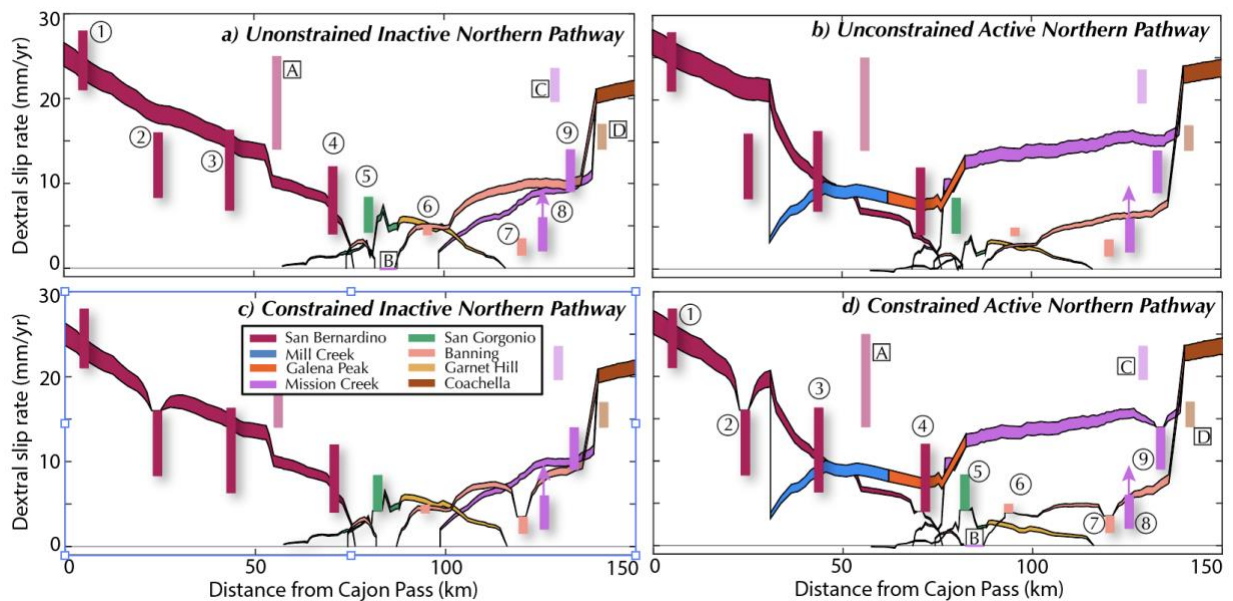


Figure 3. Dextral slip rates along strands of San Andreas fault at the upper surface of the model. Vertical bars show the geologic slip rates at sites labeled in Figure 1; bars with lighter hues are not used for the model assessment. Upward pink arrow indicates that slip rate may exceed the reported range at Thousand Palms. The shaded bands show the range of modeled strike-slip faults for the various applied tectonic loading. a) & b) show results from the unconstrained models with and without an Active Northern Pathway for slip. The *Inactive Northern Pathway* model overlaps more geologic slip rates than the *Active Northern Pathway* model. c) & d) show results for the constrained model where we prescribed strike slip rate to fit within the geologic ranges at sites with robust estimates of slip rate within the past 16,000 years.

340 The *Inactive Northern Pathway* model matches more of the geologic slip rates than the *Active Northern Pathway* model (Fig. 3 a & b). Both unconstrained models underestimate strike-slip rates at Millard Canyon (site 5) on the San Gorgonio Pass Thrust and the models overestimate slip rates at both Badger Canyon (site 2) and at Washington Street (site 7). While those are the only sites of slip rate mismatch for the *Inactive Northern Pathway* model, the *Active Northern Pathway* model has mismatch at an additional three sites. This model underestimates dextral slip
345 rate at Burro Flats (site 4) and Painted Hills (site 6) and this model overestimates dextral slip rates at Three Palms (site 9). The *Active Northern Pathway* model has much greater dextral slip along the northern pathway and underestimates dextral slip rates at all sites along the southern slip pathway, except for Washington St. (site 7).

350 In the second pair of models, we constrain the slip rates at sites where rates from the unconstrained models lie outside of the geologic ranges. The slip rates from the constrained models are pinned to the limiting value at sites that did not fall within the range in the unconstrained model. This produces sharp jumps in the dextral slip rate along faults with slip-constrained sites. For both fault configurations (Fig. 3c & d), the San Bernardino strand is pinned to the upper limit of the Badger Canyon slip rate (site 2), the San Gorgonio Pass Thrust is pinned
355 to the lower limit of the Millard Canyon dextral slip rate (site 5), and the Banning strand is pinned to the upper limit of the Washington Street slip rate (site 7). Additionally, the *Active Northern Pathway* model has pinned slip rates at the lower limits of the geologic slip rate range along the San Bernardino strand at Burro Flats (site 4) and along the Banning strand at Painted Hills (site 6). The *Active Northern Pathway* model slip rates are also pinned to the upper slip rate
360 limit along the Mission Creek strand at Three Palms (site 9).

The *Active Northern Pathway* model has greater change in slip rate with the imposed constraints than the *Inactive Northern Pathway* model. Integrating the absolute value of change in slip rate along the San Andreas fault within this study area, the *Active Northern Pathway* model has 260 m^2/yr while the *Inactive Northern Pathway* has only 160 m^2/yr of slip rate change. Constraining
365 the slip rates has the greatest impact on slip rate distribution where we have the greatest mismatch between the unconstrained model and the geologic estimates of slip rate. For example, the pinning of slip rates results in slip distribution in the constrained models that differs significantly from both unconstrained models near Washington Street (site 7). The local reduction in slip rate produces sharp gradients in slip rate both east and west of the site in both
370 the *Inactive* and *Active Northern Pathway* models. Local slip rate gradients also arise adjacent to other constrained sites. While the slip rate constraints in the *Active Northern Pathway* model

locally impact slip, these constraints do not significantly alter the partitioning of slip between the northern and southern pathways. The Mission Creek strand maintains ~15 mm/yr of slip and the strands of the southern pathway maintain ~5 mm/yr of dextral slip.

375 The *Active Northern Pathway* model is not constrained at the Mission Creek alluvial complex (site B) within Figure 3b, even though some studies have found zero slip here along the Mission Creek fault strand (Kendrick, 2015). Figure 4 provides an additional version of the constrained *Active Northern Pathway* model, which adds a constraint of zero dextral slip at the Mission Creek alluvial complex where slip rates are debated (site B). In similar manner as the other sites, 380 constraining slip rate at the Mission Creek alluvial complex produces sharp local gradients in slip rate but does not shift the partitioning of slip rate between the two pathways.

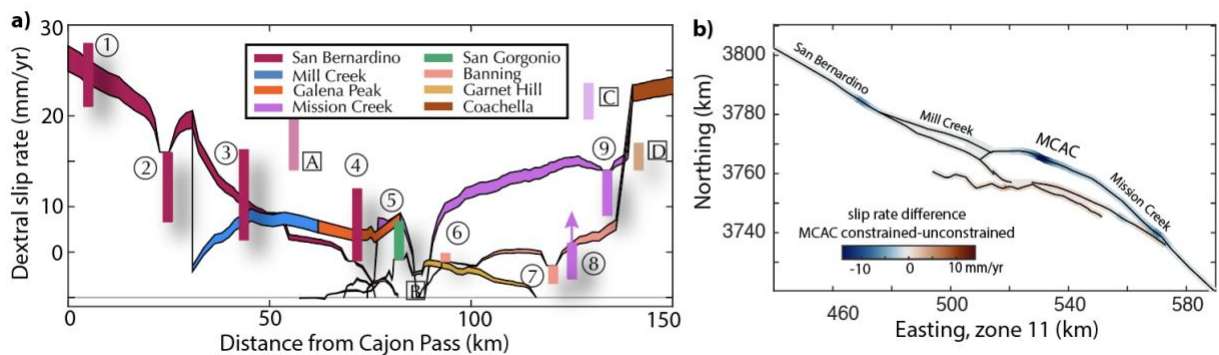


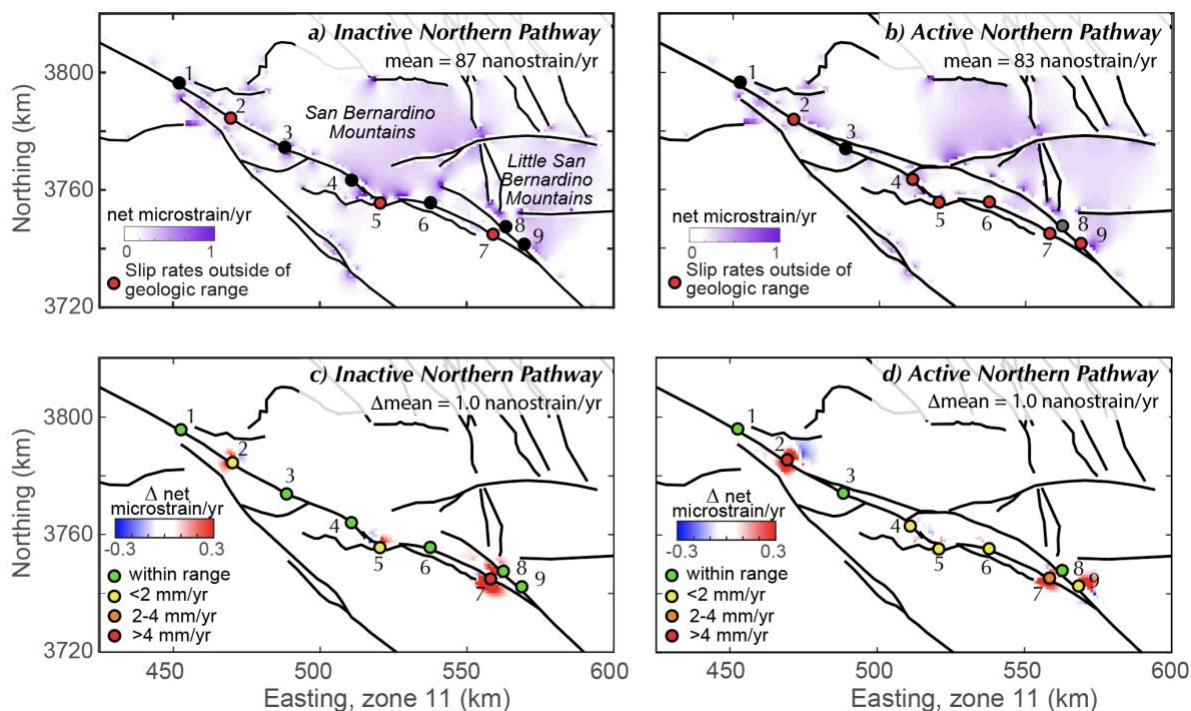
Figure 4. a) Dextral slip rates along strands of San Andreas fault at the upper surface of the model for the constrained *Active Northern Pathway* model of Figure 3d that also limits slip rate to zero at the Mission Creek alluvial complex (MCAC). Vertical bars show the geologic slip rates at sites labeled in Figure 1 - lighter hued bars are slip rates that are not used for the model assessment. b) Difference in slip rate between the constrained *Active Northern Pathway* model of Figure 3d and the model with MCAC also constrained to have zero slip.

4.2 Off-fault deformation

The net off-fault deformation rate calculated at distances greater than 1 km from active fault traces is the sum of the absolute values of dilatational and distortional strain rate components (Figure 5). Both unconstrained models that allow faults to slip everywhere in response to loading produce distributed off-fault deformation in the western San Bernardino Mountains and within the Little San Bernardino Mountains (Figure 5 a&b). In the unconstrained models of both fault configurations, localized off-fault deformation develops near many fault intersections and irregularities as strike-slip is hindered by these irregularities. Within the *Active Northern Pathway* model, the irregularities along the southern slip pathway produce lesser local off-fault deformation because the southern pathway has lesser dextral slip to drive off-fault deformation around fault irregularities in this model (Figure 4; Beyer et al., 2018). 390

The *Inactive Northern Pathway* model produces greater off-fault deformation in the southern San Bernardino Mountains than the *Active Northern Pathway* model, which includes slip along the Mill Creek, Galena Peak and western Mission Creek strands in this region. Slip along the additional active fault strands of the northern pathway reduces the local off-fault deformation. 395

The mean off-fault deformation calculated >1 km from active faults in the study area decreases with the addition of the northern slip pathway (Table 2). The lower mean off-fault deformation of
 400 the *Active Northern Pathway* model (83 nanostrain/yr) compared to the *Inactive Northern Pathway* model (87 nanostrain/yr) is consistent with the observation that adding more faults to the system generally allows for greater fault slip and less off-fault deformation (e.g., Madden, Cooke, & McBeck, 2017; McBeck, Cooke, Herbert, Maillot, & Souloumiac, 2017).



405 **Figure 5.** Net off-fault strain maps from *Inactive Northern Pathway* (a&c) and *Active Northern Pathway* (b&d) models, each with tectonic loading at midpoint of the applied range. The top row (a&b) shows strain for the unconstrained models. The bottom row (c&d) shows the difference between the unconstrained and the models where slip rates are not permitted to exceed the geologic ranges (constrained-unconstrained). Red indicates regions of increased off-fault deformation when slip rates are constrained for that fault system configuration.

When we limit the dextral strike-slip rates at sites of the geologic investigations in the models, net off-fault deformation increases near the slip rate sites (Figure 5 c&d). Sites with larger adjustments to their slip rate have greater degree and spatial extent of off-fault deformation (Fig. 5 c&d). For most sites, the off-fault deformation is centered on the site and decreases rapidly
 410 with distance. One exception is site 7 in the *Inactive Northern Pathway* model where the constrained slip rate on the Banning strand impacts off-fault deformation at the nearby Mission Creek strand. Slip here on one strand impacts the other because the faults merge both a few km south of site 7 and at depth (Figure 1). In the *Active Northern Pathway* model, site 7 does not have as large of a slip rate adjustment as within the *Inactive Northern Pathway* model so this
 415 smaller adjustment does not impact off-fault deformation along the Mission Creek strand. The

local nature of the changes in off-fault deformation are consistent with the local changes in slip rate distributions near sites with slip rate adjustments (Figure 3).

We can assess the impact of the slip rate constraints on the off-fault deformation within the region by comparing the mean net off-fault deformation of the constrained models with those
420 calculated for the unconstrained models within the study area (Figure 4 c & d). While some locations have greater or lesser absolute net off-fault strain rate than others, the mean net off-fault strain rate for both fault configurations goes up by ~ 1 nanostrain/yr when slip rates are constrained to be within the geologic slip rate range at each investigated site.

4.3 Influence of slip rate sites on each other

425 We map out the influence of slip rates at each site on other sites with a suite of models that apply 1 mm/yr of dextral slip at each slip rate site independently. The tables of Figure 6 b & c show the resulting dextral slip rate detected at each site due to 1 mm/yr dextral slip applied to the sites listed in the first column of the table. Because the Mission Creek alluvial complex site is not part of the *Inactive Northern Pathway* model, it does not have any impact within that model.

430 The influence of sites varies within the system, and nearby sites have greater influence on each other than distal sites. For example, within both the *Inactive* and *Active Northern Pathway* models, the cluster of sites within the Indio Hills (sites 7-9, C&D) have a large influence on each other (Influence Factor 0.2-0.5; Figure 6 b&c). The influence tables are slightly asymmetric indicating that the influence of slip at one site on another site is not necessarily reciprocal. For
435 example, in the *Active Northern Pathway* model, 1 mm/yr at the Plunge Creek site produces only 0.06 mm/yr at Badger Canyon while 1 mm/yr at Badger Canyon produces 0.10 mm/yr at Plunge Creek. In other words, changes in slip at Badger Canyon have greater influence at Plunge Creek than vice versa in this model. The site influences between the Badger Canyon and Plunge Creek sites are more symmetric in the *Inactive Northern Pathway* model, which suggests that the
440 presence of the fault branch between Badger Canyon and Plunge Creek in the *Active Northern Pathway* model, reduces the influence of dextral slip at Plunge creek on Badger Canyon. The additional active northern strand also changes the influence of the Wilson Creek site between the *Active* and *Inactive Northern Pathway* models. Most other sites have similar influences on each other between the two models.

445 The influence of sites on each other generally decreases with distance between sites (Figure 6d). The best fitting exponential curve through the results shows small influence among sites farther than 20 km. In addition to this trend, some sites within 5-20 km of each other have anomalously low and high influence. Three pairs of sites with relatively low influence (1- Burro Flats & Millard Canyon; 2- Mission Creek alluvial complex & Painted Hills; 3- Washington Street &
450 Thousand Palms) are highlighted in blue on Figures 6a and 6d while three pairs of sites with relatively high influence (1 - Cajon Creek & Badger Canyon; 2- Plunge Creek & Wilson Creek; 3- Thousand Palms & Three Palms) are highlighted in red on Figures 6a and 6d. For example, the Badger Canyon and Cajon Creek sites have similar distance (19 km) as the Burro Flats and

Painted Hills sites (19 km) but have much larger influence on each other ($\sim 0.12 > 0.01$). The
455 three pairs of low influence sites for their distances all occur on different segments or parallel
branches of the fault system. Even though the sites are nearby one another, slip at one doesn't
influence slip on the nearby site because of the lack of fault connectivity at these distances. Pairs
of sites on branched faults that are sited very close to the branch, such as Washington Street and
Thousand Palms, have influence consistent with the general trend on Figure 6d because slip at
460 one of these sites is close enough to where the faults intersect that slip on one branch can
influence the nearby branch. The pairs of sites that have relatively high influence for their
distances all occur along continuous portions of the fault without branches, segments, or kinks.
Dextral slip transmits more easily along the continuous segments so that slip at one site has a
high influence on other sites along the continuous segment.

465

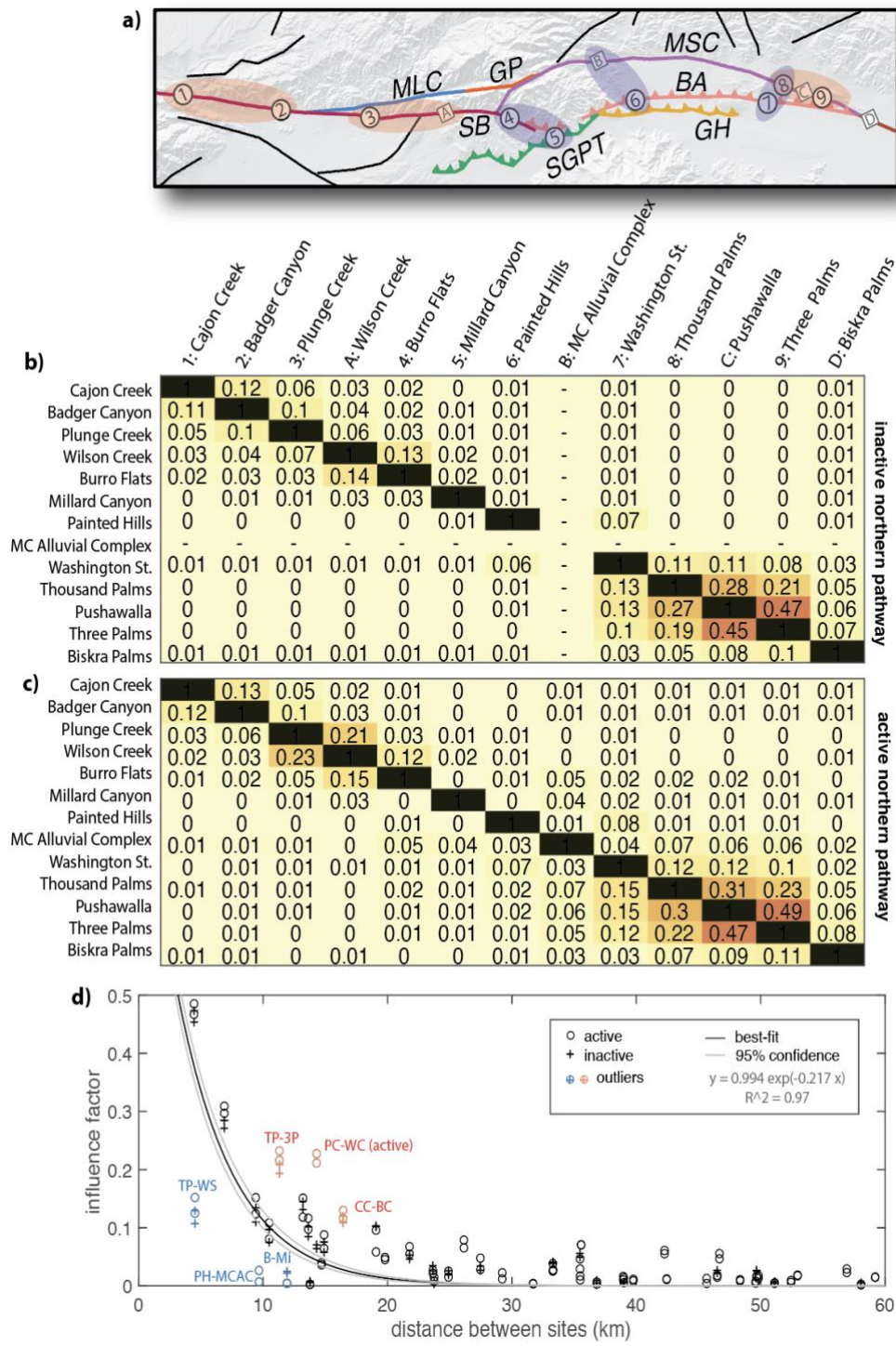


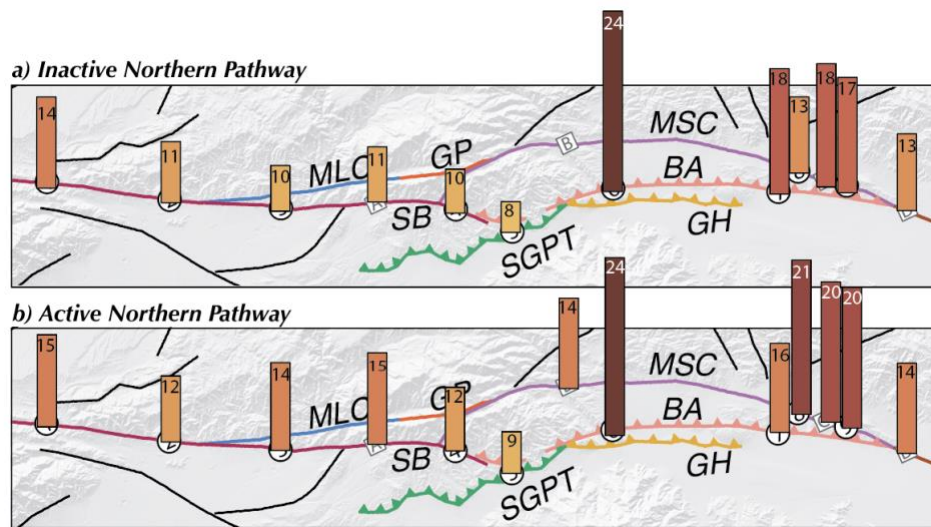
Figure 6. Influence of 1 mm/yr dextral slip applied at sites listed at left on all other sites in the model. a) Map of the site locations with ellipses highlighting pairs of sites with relative high influence (red) and low influence (blue). b) and c) influence for *Inactive Northern Pathway* and *Active Northern Pathway* models respectively. The diagonals of the table are all 1%, reflecting the influence of each site on itself while the off-diagonals show influence values less than one. d) Correlation of influence factor with distance between sites shows that sites have greater influence on nearby sites. Lines show an exponential best fit to all the data. Outliers to the

best fit are highlighted in red and blue. TP - Thousand Palms; 3P - Three Palms; PC - Plunge Creek; WC - Wilson Creek; CC-Cajon Creek; BC- Badger Canyon; WS = Washington Street; PH = Painted Hills; MCAC - Mission Creek Alluvial Complex; B = Burro Flats; Mi = Millard Canyon.

4.4 Impact of each slip rate site on the fault system

While Figure 6 shows how each site influences slip rate at other sites, that analysis does not inform the impact of the sites' slip rates on the stretches of fault between the sites. To assess this, we map the dextral slip in response to the applied 1 mm/yr at each site and integrate the slip along the faults to derive the total impact factor (Figure 7). The piecewise integration excludes the patch with applied slip and excludes regions with less than 2% of the applied slip (slip < 0.02 mm/yr). In this study, we only constrained slip for the upper 2 km of the fault surface. If these patches were extended to greater depths, we would see greater values for the impact factors among sites and on the system, but the relative impact may be similar.

The *Inactive Northern Pathway* and *Active Northern Pathway* models show similar patterns of fault slip for most sites (Figure 7). The impact factors of the sites range from 8 to 24. The lowest impact factor (IF) is at the Millard Canyon site for both model geometries. Sites along the San Bernardino strand in the *Inactive Northern Pathway* model also have relatively low impact factors. The application of 1 mm/yr of slip at these sites produces less fault slip than the other sites, implying that this applied slip produces greater off-fault deformation. For Millard Canyon, off-fault deformation may arise because the site is located within a segmented portion of the southern San Andreas fault, along the San Gorgonio Pass Thrust, which does not at the surface meet with the San Bernardino strand. This segmentation leads to greater off-fault deformation in this region.



485

Figure 7. Slip rate impact factors for both the a) *Inactive Northern Pathway* and b) *Active Northern Pathway* models. The darkness and height of the bar represent the impact factor value of each site.

The Painted Hills site, which has low influence on other sites (Figure 6) has the greatest impact factor of all of the sites (Figure 7). Because this site sits on the Banning strand, which merges with the parallel-striking Garnet Hill strand at depth, slip rates imposed on the Banning strand

490 also impact slip rates on the Garnet Hill strand. The plots of slip distribution on Figure 8 show
how slip applied at Painted Hills impacts nearby fault strands. The Garnet Hill strand doesn't yet
have any slip rates sites, so the interaction of the Banning and Garnet Hill strands was not
considered in the site analysis of Figure 6. The Washington Street site also occurs along the
Banning strand but has a lower impact factor than the Painted Hills site because the Garnet Hill
495 strand is not active that far east. Furthermore, while the Banning strand merges at depth to the
Mission Creek strand at the Washington Street site, these two faults meet much deeper than the
Garnet Hill and Banning faults (Figure 1), so the transmission of dextral slip at the Earth's
surface is not as efficiently transmitted as between the Banning and Garnet Hills strands at the
Painted Hills site.

500 Due to the longer active fault trace in the *Active Northern Pathway* model, slip from the
Washington Street site as well as slip from sites along the Mission Creek strand and Coachella
segment extends much farther northwest along the Mission Creek strand than in the *Inactive
Northern Pathway* model (Figure 8). This increase in slip extent with the *Active Northern
Pathway* model also increases the impact factor of most of the sites. This is most notable for the
Mission Creek alluvial complex; while this site does not have a high impact factor, slip applied
505 to this location induces slip along many parts of the fault system.

The impact factor also increases at sites along the San Bernardino strand with addition of the
northern slip pathway to host dextral slip. The Plunge Creek and Wilson Creek sites have the
greatest increase of 4 between the *Inactive* and *Active Northern Pathway* models. The close
branch angle between the San Bernardino and Mill Creek strands ($\sim 10^\circ$) allows dextral slip
510 applied along one branch to produce shear tractions on the other branch that increase the impact
factor compared to the model without the branch.

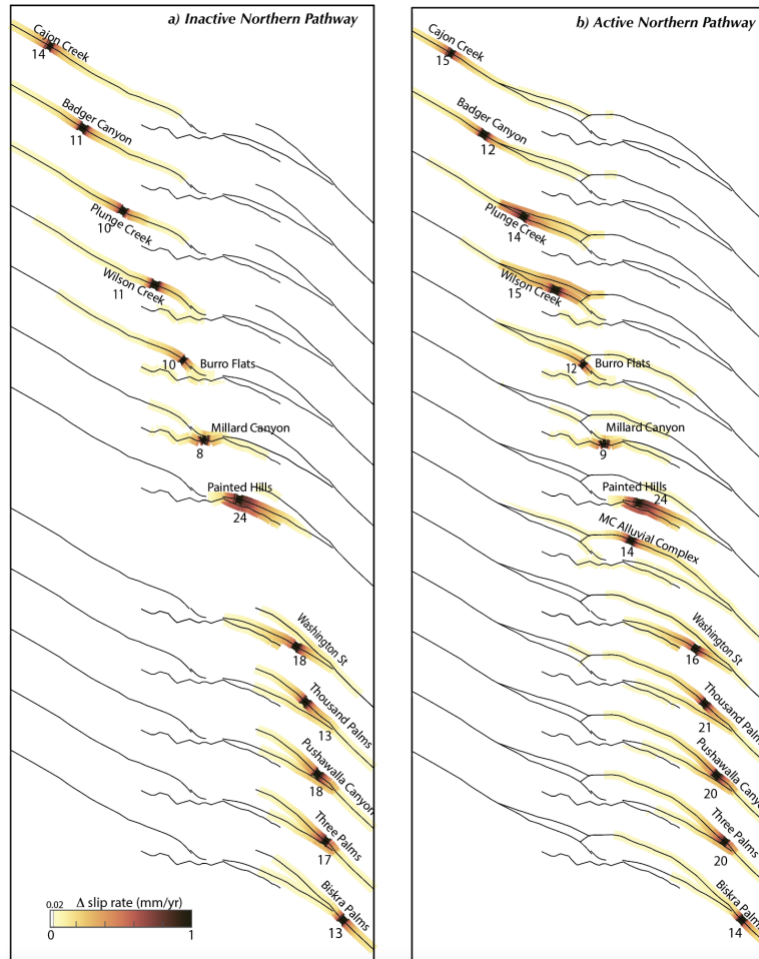


Figure 8. Distribution of dextral slip distribution $>2\%$ of the applied slip at each site within the a) *Inactive Northern Pathway* and b) *Active Northern Pathway* models. Numbers report the integrated impact factor along the faults (IF in m^2/yr).

515 The impact factor of sites along branches is greater than the impact factor of sites outside of the
 branch (e.g. Badger Canyon) because slip on one branch impacts the other to increase the impact
 of sites within the branch. For example, in the *Active Northern Pathway* model, the impact factor
 of the Plunge Creek and Wilson Creek sites is greater than that of the Badger Canyon site, north
 of the branch of the San Bernardino strand with the Mill Creek Strand. Also in both models, sites
 520 along the Mission Creek and Banning strands have greater impact factors than the Biskra Palms
 site, which is located south of the merger of the Banning and Mission Creek strands.

5 Discussion

The results of this study and that of Beyer et al. (2018) show that adding a northern pathway for
 fault slip modifies slip distribution. While it is agreed that the Mission Creek strand is active near
 525 its intersection with the Banning strand, debate persists on the activity of the northern pathway
 near and northwest of the Mission Creek alluvial complex (Beyer et al., 2018; Fosdick &
 Blisniuk, 2018; Kendrick et al., 2015). This study is not able to ascertain between the two viable

models. On the one hand, the *Inactive Northern Pathway* model produces slip rates that match more of the geologic slip rates. On the other hand, the *Inactive Northern Pathway* model
530 produces greater off-fault deformation in the region of the Mill Creek fault, which can promote slip on this structure. Alternatively, the accrued off-fault deformation could be consumed by inelastic processes within the crust, such as pressure solution creep (e.g., Gratier, Renard, & Labaume, 1999), without promoting fault slip. Without independent data to confirm the rate of off-fault deformation within the San Gorgonio Pass, we don't know if the accumulation of this
535 strain is reasonable or if it supports the interpretation of active slip along the Mill Creek fault.

5.1 Incompatibility of slip rates and fault geometry

Where the mechanical model produces slip rates that are consistent with the geologic observations, we can say that the tested fault geometry is mechanically and kinematically compatible with the slip rates. However, regions where slip rates from the numerical model do
540 not agree with geologic estimates may have incompatibility between the tested fault geometry and slip rate. In the models with constrained slip rates, this incompatibility produces increased off-fault deformation (Figure 5). For both the unconstrained and the constrained models, the *Active Northern Pathway* model produces lesser off-fault deformation than the *Inactive Northern Pathway* model because the addition of the Mill Creek strand provides an additional opportunity
545 for accommodation of strain as fault slip rather than off-fault deformation.

Little to no increase in off-fault deformation occurs where the unconstrained model fault slip rates are within or near the limits of the geologic ranges. The compatibility of dextral slip rates with interpreted fault geometry doesn't preclude the possibility that the models inaccurately represent the subsurface fault configuration. For example, geophysical evidence suggests that
550 rather than the vertical dip represented in this study, the San Bernardino strand may dip to the north east (Fuis, Scheirer, Langenheim, & Kohler, 2012). Both vertical and dipping faults can accommodate strike slip so that variations in fault dip might not produce distinguishable dextral slip rates (e.g., Fattaruso et al., 2014). Additionally, some ranges in geologic slip rates are large enough that several alternative fault configurations might all match within the slip rate ranges.

Regions with mismatched slip rates, such as the Indio Hills and near Badger Canyon, indicate that slip rates in these regions may be kinematically incompatible with the interpreted fault geometry. These incompatibilities highlight the need for additional constraints on subsurface active fault configuration in these regions. While microseismicity during the interseismic period can illuminate subsurface active fault geometry, such as along the San Jacinto fault (Ross,
560 Hauksson, & Ben-Zion, 2017), the San Andreas fault has little microseismicity. Uncertainty persists on the subsurface geometry of active faults in these regions. For example, at Cajon Pass, the San Andreas and San Jacinto faults may be connected at depth even though the surface traces are separated by several km (e.g., Matti & Morton, 1993; McGill et al., 2013). A hard connection at depth between these faults would alter slip distribution among the faults. Mechanical models
565 of Herbert et al. (2014) show that connecting the San Jacinto and San Andreas faults reduces

dextral slip rates at the Badger Canyon site, which would better match the site's geologic slip rates.

570 Near the Indio Hills, the Banning and Mission Creek strands merge into the Coachella segment of the San Andreas fault. The subsurface geometry of the faults near this intersection is not well constrained (e.g., Fuis et al., 2017). The off-fault deformation in this region and the mismatch to geologic slip estimates (Figure 5) could be a result of incorrectly inferred fault geometry.

5.2 High and low impact structural positions along the fault system

575 The impact factor of sites depends on structural position and even sites close to each other may have very different impact on the deformation of the fault system (Figure 7). Sites along parallel or subparallel branched fault segments, such as Painted Hills and Plunge Creek in the *Active Northern Pathway* model, have greater impact on the fault system than sites outside of the branch because slip is transmitted between connected parallel fault segments. At the same time sites along unconnected strands or near intersecting faults that are not parallel or subparallel, such as Burro Flats and Millard Canyon, have low impact factor. At these sites, the complex fault 580 geometry produces greater off-fault deformation (Figures 5a & 5b).

585 The geologic slip rates have large uncertainties much larger than the 1 mm/yr applied to the slip rates in the assessment of the sites' impact. Small changes of slip rate within the slip rate uncertainty at some sites of geologic slip rate investigation can have a large impact on the partitioning of deformation within the fault system. Along planar strike-slip faults, different sites may have similar impact on the system; however, the complex geometry of the San Andreas fault through the San Gorgonio Pass means that the impact of slip rate varies greatly with structural position. Slip rate sites along fault branches necessitate detailed consideration because these are areas with high impact factors, as slip on one branch impacts slip along the other.

590 Older slip rates that do not use modern methods of dating landforms, could benefit from re-dating. For example, the age of the alluvial fan at Wilson Creek is estimated from soil chronology (Harden & Matti, 1989). Because this site is located near a fault branch, a refined slip rate estimate here, as well as additional slip rate sites along the northern pathway, could provide substantial improvement to our understanding of strain partitioning and potential activity of the Mill Creek strand of the San Andreas.

595 Sites along irregular or disconnected faults have a low impact factor but also have greater nearby off-fault deformation. For example, the Burro Flats and Millard Canyon sites are along relatively disconnected fault strands so that they have both low influence on other sites (Figure 6) and low impact on the nearby fault system (Figures 7&8). Slip at these sites contributes to off-fault deformation, instead of being transmitted along the fault system. The local accumulation of off- 600 fault deformation may promote distributed inelastic deformation or the development of new or reactivation of old fault structures.

5.3 Seismic hazard

The numerical models demonstrate the high spatial variability of strike-slip rates along faults with non-planar configuration. The southern San Andreas fault is one of the most thoroughly investigated fault systems in the world; most restraining bends and branches along strike-slip faults have far fewer slip rate data than this fault system. If seismic hazard estimates use a single rate to represent slip rates through a complex restraining bend, they might miss the spatial variations of strike-slip rate. Strike-slip fault branches show particularly high spatial variability of slip rate (Figure 3), accrual of nearby off-fault deformation (Figure 5) and impact on the fault system (Figures 7 and 8). Fault branches warrant detailed investigation in order to best understand regional strain partitioning. Furthermore, the range of impact factors for the different sites demonstrates that not all slip rate sites have equal impact. Consequently, if we have errors or are off in our estimate of slip rate at any one of the more sensitive sites, this error may have a large impact on our understanding of the deformation of the fault system and thus hinder our ability to accurately assess seismic hazard in the region.

7 Conclusions

We use three-dimensional numerical crustal deformation models to analyze the role of slip rate sites in determining deformation of the southern San Andreas fault system within the San Gorgonio Pass region. We investigate the compatibility of models with and without active slip along the northern pathway of the San Andreas fault around the San Gorgonio Pass with geologic slip rates. Within unconstrained models that allow all faults to slip freely everywhere in response to tectonic loading and fault interaction, the *Active Northern Pathway* model produces slip rates with greater mismatch to rates within the past 16 k years at sites of geologic investigations than the *Inactive Northern Pathway* model. To assess incompatibilities between fault geometry and slip rate, we utilize a new approach and constrain the slip rates along the faults to within the geologic range at each geologic slip rate site. Slip rate adjustments in the constrained model ensure that the model matches all geologic slip rates, but this produces local off-fault deformation near the constrained sites.

Maps of off-fault deformation show that the *Inactive Northern Pathway* fault configuration for both the unconstrained and the constrained models has greater off-fault deformation than the *Active Northern Pathway*. The additional northern slip pathway provides an opportunity for a greater amount of deformation to be expressed as fault slip. While fault systems may evolve to reach more efficient configurations (e.g., Hatem et al., 2017; McBeck et al., 2017), this does not mean that the presently active configuration must be the most optimal. Additional slip rate constraints and data off-fault deformation rates within the southern San Andreas system would provide valuable information to assess between the two alternative configurations.

We assess how much of an impact the incompatibilities between fault geometry and geologic slip rate have on the system by assessing the impact of slip rate changes. Small changes of slip rate at any one site of geologic slip rate investigation impact slip rates elsewhere in the system.

640 However, this impact is not the same for all sites, which means that inaccuracies in the slip rate
that we use for seismic hazard analysis may have differing impact along active fault systems at
one site than another. The degree of impact that slip rate sites have on the fault system depends
on their structural positions. Sites along segmented faults may have lesser impact than sites along
645 a continuous fault segment, and sites along fault branches have the greatest impact. Fault
branches along strike-slip faults require detailed investigation because these areas have high
spatial variability of slip rate and can impact the nearby branches of the fault system, adding
additional uncertainty to our current assessment of the seismic hazard.

Acknowledgements

This research was partially supported by the Southern California Earthquake Center
650 (Contribution No. 11878). SCEC is funded by NSF Cooperative Agreement EAR-1600087 &
USGS Cooperative Agreement G17AC00047.

Data and code availability

The crustal deformation software Poly3D is made available by the Stanford tectonic
geomorphology lab at <https://github.com/stgl/poly3d>. Input files for the unconstrained and
655 constrained Active Northern Pathway and Inactive Northern Pathway models used in this study
can be downloaded from doi:10.6084/m9.figshare.20274363.

Competing interests

The authors have no competing interests.

References

- 660 Becker, T. W., Hardebeck, J. L., & Anderson, G. (2005). Constraints on fault slip rates of the
southern California plate boundary from GPS velocity and stress inversions. *Geophysical
Journal International*, 160(2), 634–650. <https://doi.org/10.1111/j.1365-246X.2004.02528.x>
- Behr, W. M., Rood, D. H., Fletcher, K. E., Guzman, N., Finkel, R., Hanks, T. C., ... Yule, J. D.
665 (2010). Uncertainties in slip-rate estimates for the Mission Creek strand of the southern San
Andreas fault at Biskra Palms Oasis, southern California. *Bulletin of the Geological Society
of America*, 122(9–10), 1360–1377. <https://doi.org/10.1130/B30020.1>
- Beyer, J. L., Cooke, M. L., & Marshall, S. T. (2018). Sensitivity of deformation to activity along
the Mill Creek and Mission Creek strands of the southern San Andreas fault. *Geosphere*,
14(6), 2296–2310. <https://doi.org/10.1130/GES01666.1>
- 670 Blisniuk, K., Scharer, K., Sharp, W. D., Burgmann, R., Amos, C., & Rymer, M. (2021). A
revised position for the primary strand of the Pleistocene-Holocene San Andreas fault in
southern California. *Science Advances*, 7(13). <https://doi.org/10.1126/sciadv.aaz5691>
- Cooke, M. L., & Dair, L. C. (2011). Simulating the recent evolution of the southern big bend of
675 the San Andreas fault, Southern California. *Journal of Geophysical Research: Solid Earth*,
116(4). <https://doi.org/10.1029/2010JB007835>

- Cooke, M. L., Schottenfeld, M. T., & Buchanan, S. W. (2013). Evolution of fault efficiency at restraining bends within wet kaolin analog experiments. *Journal of Structural Geology*, *51*, 180–192. <https://doi.org/10.1016/j.jsg.2013.01.010>
- 680 Cooke, M. L., Toeneboehn, K., & Hatch, J. L. (2020). Onset of slip partitioning under oblique convergence within scaled physical experiments. *Geosphere*, *16*(X), 1–15. <https://doi.org/10.1130/ges02179.1>
- Crider, J. G., & Pollard, D. D. (1998). Fault linkage: Three-dimensional mechanical interaction between echelon normal faults. *Journal of Geophysical Research*, *103*391(10), 373–24. <https://doi.org/10.1029/98JB01353>
- 685 Dawers, N. H., & Anders, M. H. (1995). Displacement-length scaling and fault linkage. *Journal of Structural Geology*, *17*(5), 607–614.
- DeMets, C., Gordon, R. G., & Argus, D. F. (2010). Geologically current plate motions. *Geophysical Journal International*, *181*(1), 1–80. <https://doi.org/10.1111/j.1365-246X.2009.04491.x>
- 690 Di Toro, G., Hirose, T., Nielsen, S. B., & Pennacchioni, G. (2006). Natural and Experimental Evidence During Earthquakes, *311*(February), 647–649.
- Dibblee, T. W. (1964). *Geologic map of the San Gorgonio Mountain quadrangle, San Bernardino and Riverside Counties, California*. US Geological Survey.
- 695 Elston, H., Cooke, M., & Hatem, A. (2022). Non-steady-state slip rates emerge along evolving restraining bends under constant loading. *Geology*, *50*(5), 532–536. <https://doi.org/10.1130/G49745.1>
- Fattaruso, L. A., Cooke, M. L., & Dorsey, R. J. (2014). Sensitivity of uplift patterns to dip of the San Andreas fault in the Coachella Valley, California. *Geosphere*, *10*(6). <https://doi.org/10.1130/GES01050.1>
- 700 Fattaruso, L. A., Cooke, M. L., Dorsey, R. J., & Housen, B. A. (2016). Response of deformation patterns to reorganization of the southern San Andreas fault system since ca. 1.5i½Ma. *Tectonophysics*, *693*, 474–488. <https://doi.org/10.1016/j.tecto.2016.05.035>
- 705 Fay, N. P., & Humphreys, E. D. (2005). Fault slip rates, effects of elastic heterogeneity on geodetic data, and the strength of the lower crust in the Salton Trough region, southern California. *Journal of Geophysical Research: Solid Earth*, *110*(9), 1–14. <https://doi.org/10.1029/2004JB003548>
- Fosdick, J. C., & Blisniuk, K. (2018). Sedimentary signals of recent faulting along an old strand of the San Andreas Fault, USA. *Scientific Reports*, *8*(1), 12132.
- 710 Fuis, G. S., Bauer, K., Goldman, M. R., Ryberg, T., Langenheim, V. E., Scheirer, D. S., ... Aagaard, B. (2017). Subsurface geometry of the san andreas fault in southern California: Results from the salton seismic imaging project (SSIP) and strong ground motion expectations. *Bulletin of the Seismological Society of America*, *107*(4), 1642–1662. <https://doi.org/10.1785/0120160309>
- 715 Fuis, G. S., Scheirer, D. S., Langenheim, V. E., & Kohler, M. D. (2012). A new perspective on the Geometry of the San Andreas fault in southern California and its relationship to

Lithospheric structure. *Bulletin of the Seismological Society of America*, 102(1), 236–251. <https://doi.org/10.1785/0120110041>

- 720 Fumal, T. E., Rymer, M. J., & Seitz, G. G. (2002). Timing of large earthquakes since A.D. 800 on the Mission Creek strand of the San Andreas fault zone at Thousand Palms Oasis, near Palm Springs, California. *Bulletin of the Seismological Society of America*, 92(7), 2841–2860. <https://doi.org/10.1785/0120000609>
- Gabrielov, a, Keilis-Borok, V., & Jackson, D. D. (1996). Geometric incompatibility in a fault system. *Proceedings of the National Academy of Sciences of the United States of America*, 93(9), 3838–3842. <https://doi.org/10.1073/pnas.93.9.3838>
- 725 Gold, P. O., Behr, W. M., Rood, D., Sharp, W. D., Rockwell, T. K., Kendrick, K., & Salin, A. (2015). Holocene geologic slip rate for the Banning strand of the southern San Andreas Fault, southern California. *Journal of Geophysical Research: Solid Earth*, 120(8), 5639–5663.
- 730 Goldsby, D. L., & Tullis, T. E. (2011). Flash heating leads to low frictional strength of crustal rocks at earthquake slip rates. *Science*, 334(6053), 216–218.
- Gratier, J.-P., Renard, F., & Labaume, P. (1999). How pressure solution creep and fracturing processes interact in the upper crust to make it behave in both a brittle and viscous manner. *Journal of Structural Geology*, 21(8–9), 1189–1197.
- 735 Harden, J., & Matti, J. (1989). Holocene and late Pleistocene slip rates on the San Andreas fault in Yucaipa, California, using *Bulletin of the Geological Society of America*, (September), 1107–1117. [https://doi.org/10.1130/0016-7606\(1989\)101<1107](https://doi.org/10.1130/0016-7606(1989)101<1107)
- Hatem, A. E., Cooke, M. L., & Madden, E. H. (2015). *Journal of Geophysical Research : Solid Earth*, 1–18. <https://doi.org/10.1002/2014JB011735>.Received
- 740 Hatem, A. E., Cooke, M. L., & Toeneboehn, K. (2017). Strain localization and evolving kinematic efficiency of initiating strike-slip faults within wet kaolin experiments. *Journal of Structural Geology*, 101, 96–108. <https://doi.org/10.1016/j.jsg.2017.06.011>
- Heermance, R. V., & Yule, D. (2017). Holocene slip rates along the San Andreas Fault System in the San Gorgonio Pass and implications for large earthquakes in southern California. *Geophysical Research Letters*, 44(11), 5391–5400. <https://doi.org/10.1002/2017GL072612>
- 745 Herbert, J.W., Cooke, M. L., & Marshall, S. T. (2014). Influence of fault connectivity on slip rates in southern California: Potential impact on discrepancies between geodetic derived and geologic slip rates. *Journal of Geophysical Research: Solid Earth*, 119(3). <https://doi.org/10.1002/2013JB010472>
- 750 Herbert, Justin W., & Cooke, M. L. (2012). Sensitivity of the Southern San Andreas fault system to tectonic boundary conditions and fault configurations. *Bulletin of the Seismological Society of America*, 102(5). <https://doi.org/10.1785/0120110316>
- 755 Kendrick, K. J., Matti, J. C., & Mahan, S. A. (2015). Late quaternary slip history of the Mill Creek strand of the San Andreas fault in San Gorgonio Pass, southern California: The role of a subsidiary left-lateral fault in strand switching. *Bulletin of the Geological Society of America*, 127(5–6), 825–849. <https://doi.org/10.1130/B31101.1>

- Lin, G. (2013). Three-dimensional seismic velocity structure and precise earthquake relocations in the Salton trough, southern California. *Bulletin of the Seismological Society of America*, 103(5), 2694–2708.
- 760 Lindsey, E. O., & Fialko, Y. (2013). Geodetic slip rates in the southern San Andreas Fault system: Effects of elastic heterogeneity and fault geometry. *Journal of Geophysical Research: Solid Earth*, 118(2), 689–697. <https://doi.org/10.1029/2012JB009358>
- Madden, E. H., Cooke, M. L., & McBeck, J. (2017). Energy budget and propagation of faults via shearing and opening using work optimization. *Journal of Geophysical Research: Solid Earth*, 122(8). <https://doi.org/10.1002/2017JB014237>
- 765 Marshall, S. T., Cooke, M. L., & Owen, S. E. (2009). Interseismic deformation associated with three-dimensional faults in the greater Los Angeles region, California. *Journal of Geophysical Research: Solid Earth*, 114(12). <https://doi.org/10.1029/2009JB006439>
- 770 Matti, J. C., & Morton, D. M. (1993). Paleogeographic evolution of the San Andreas fault in southern California: A reconstruction based on a new cross-fault correlation. *The San Andreas Fault System: Displacement, Palinspastic Reconstruction, and Geologic Evolution*, 107–159. <https://doi.org/10.1130/MEM178-p107>
- Matti, J. C., Morton, D. M., & Cox, B. F. (1985). *Distribution and geologic relations of fault systems in the vicinity of the central Transverse Ranges, southern California*. US Geological Survey.
- 775 McBeck, J. A., Cooke, M. L., Herbert, J. W., Maillot, B., & Souloumiac, P. (2017). Work Optimization Predicts Accretionary Faulting: An Integration of Physical and Numerical Experiments. *Journal of Geophysical Research: Solid Earth*, 122(9), 7485–7505. <https://doi.org/10.1002/2017JB013931>
- 780 McGill, S. F., Owen, L. A., Weldon, R. J., & Kendrick, K. J. (2013). Latest pleistocene and holocene slip rate for the San Bernardino Strand of the San Andreas Fault, Plunge Creek, Southern California: Implications for strain partitioning within the Southern San Andreas Fault system for the last ~35 k.y. *Bulletin of the Geological Society of America*, 125(1–2), 48–72. <https://doi.org/10.1130/B30647.1>
- 785 McGill, S. F., Owen, L. A., Weldon, R. J., Kendrick, K. J., & Burgette, R. J. (2021). Latest Quaternary slip rates of the San Bernardino strand of the San Andreas fault, southern California, from Cajon Creek to Badger Canyon. *Geosphere*, 17(5), 1354–1381. <https://doi.org/10.1130/GES02231.1>
- 790 McPhillips, D., & Scharer, K. M. (2018). Quantifying Uncertainty in Cumulative Surface Slip Along the Cucamonga Fault, a Crustal Thrust Fault in Southern California. *Journal of Geophysical Research: Solid Earth*, 123(10), 9063–9083. <https://doi.org/10.1029/2018JB016301>
- Meade, B. J., & Hager, B. H. (2005). Block models of crustal motion in southern California constrained by GPS measurements. *Journal of Geophysical Research: Solid Earth*, 110(3), 1–19. <https://doi.org/10.1029/2004JB003209>
- 795 Muñoz Zapata, J. J. (2017). Holocene geologic slip rate for the Mission Creek strand of the southern San Andreas fault, Indio Hills.

- Orozco, A. A. (2004). Offset of a mid-Holocene alluvial fan near Banning, CA: Constraints on the slip rate of the San Bernardino strand of the San Andreas Fault. California State University, Northridge.
- 800 Plesch, A., Shaw, J. H., Benson, C., Bryant, W. A., Carena, S., Cooke, M., ... Yeats, R. (2007). Community Fault Model (CFM) for southern California. *Bulletin of the Seismological Society of America*, 97(6). <https://doi.org/10.1785/0120050211>
- Ross, Z. E., Hauksson, E., & Ben-Zion, Y. (2017). Abundant off-fault seismicity and orthogonal structures in the San Jacinto fault zone. *Science Advances*, 3(3).
805 <https://doi.org/10.1126/sciadv.1601946>
- Sharp, R. V. (1981). Variable rates of late Quaternary strike slip on the San Jacinto fault zone, southern California. *Journal of Geophysical Research*, 86(B3), 1754–1762.
<https://doi.org/10.1029/JB086iB03p01754>
- 810 Shaw, J. H., Plesch, A., Tape, C., Suess, M. P., Jordan, T. H., Ely, G., ... Munster, J. (2015). Unified Structural Representation of the southern California crust and upper mantle. *Earth and Planetary Science Letters*, 415, 1–15. <https://doi.org/10.1016/j.epsl.2015.01.016>
- Stanford tectonic geomorphology lab. (n.d.). Poly3D. Retrieved from
<https://github.com/stgl/poly3d>
- 815 Thomas, A. (1993). Poly3D: A three-dimensional, polygonal element, displacement boundary element computer program with applications to fractures, faults, and cavities in the Earth's crust [MS thesis].
- Weldon, R. J., & Sieh, K. E. (1985). Holocene rate of slip and tentative recurrence interval for large earthquakes of the San Andreas fault, Cajon Pass, southern California. *Geological Society of America Bulletin*, 96(6), 793–812. [https://doi.org/10.1130/0016-7606\(1985\)96<793:HROSAT>2.0.CO;2](https://doi.org/10.1130/0016-7606(1985)96<793:HROSAT>2.0.CO;2)
820
- Yang, W., Hauksson, E., & Shearer, P. M. (2012). Computing a large refined catalog of focal mechanisms for southern California (1981-2010): Temporal stability of the style of faulting. *Bulletin of the Seismological Society of America*, 102(3), 1179–1194.
<https://doi.org/10.1785/0120110311>
- 825 Yule, D., & Sieh, K. (2003). Complexities of the San Andreas fault near San Geronio Pass: Implications for large earthquakes. *Journal of Geophysical Research*, 108(B11), 2548.
<https://doi.org/10.1029/2001JB000451>